Chapter 2
Thermal Conductivity Measurements in 2D Materials

Abstract Measuring the thermal conductivity of materials is a very important field as the continuation of the improvement in modern electronics and optoelectronics heavily depends on the thermal management. Both high thermal conductivity and low thermal conductivity materials are required in the device design. Besides the fields mentioned above, excess heat scavenging via thermoelectric devices is an ever-growing field. Thermoelectric devices performance is determined by the figure of merit $Z = S^2\sigma\kappa$ where S is the Seebeck coefficient, σ is the electrical conductivity and κ is the thermal conductivity. Materials that are good electrical conductors and thermal insulators are needed for efficient thermoelectric devices.

Keywords Thermal conductivity theory · Thermal conductivity measurement methods · Raman thermometry · Micro-bridge thermometry · Time-domain thermoreflectance · Bolometric thermal conductivity measurements

2.1 Introduction to Thermal Conductivity and Thermal Conductivity Measurement Techniques

After the advent of the graphene in 2004, the study of the solid-state phenomena is revolutionized as the atomically thin materials become widely available. Mechanically exfoliated monolayers of many two-dimensional materials revealed plethora of phenomena and enabled the possibility of novel electronics and optoelectronics applications due to the new electronic degrees of freedom that can be relatively easily studied. A further dimension in the study of the atomically thin materials has been introduced via stacking of various monolayers to achieve new functionality. All these developments in the field have led to the proof-of-concept demonstrations at the prototype level. Although, there is not enough incentive for the industry to adopt these newly discovered materials yet, with the recent developments in the large area high quality synthesis of the 2D materials within a decade or so they most likely compliment the engineering materials. An integral part of this process is the measurement of the thermal conductivity values in 2D materials starting from a few monolayers down to the single layer limit as well as their heterostructures to aid the engineering of the high-performance devices.

T. S. Kasirga, *Thermal Conductivity Measurements in Atomically Thin Materials and Devices*, Nanoscience and Nanotechnology,
https://doi.org/10.1007/978-981-15-5348-6_2

The challenge in measuring the thermal conductivity in atomically thin materials is self-evident. As we will discuss in the following parts, thermal conductivity measurements in bulk materials and even in thin films is relatively easier due to the large lateral sizes. At its current stage, most 2D materials can only be obtained as crystals of a few tens of micrometers in-plane direction. This challenge in handling of the samples complicated the measurement methods and decreases the accuracy of the temperature profiling of the samples as well as the heat measurements. Thus, many measurement techniques fail to measure the thermal conductivity precisely. In this chapter, I will introduce thermal conductivity in solid media and common methods used to measure thermal conductivity. Before proceeding with the methods, I would like to provide a brief introduction to thermal conduction in solid media.

2.2 Thermal Conductivity in Solid Media

Thermal conductivity is a measure of the ability to transfer heat spatially in a material. The heat flux from the hotter side of the material to its colder side is proportional to the temperature gradient over a material through the negative of the thermal conductivity by the Fourier's law. A general formulation of the Fourier's law can be written as:

$$\mathbf{Q}(\mathbf{r}, t) = -\kappa \nabla T(\mathbf{r}, t) \tag{2.1}$$

where $\mathbf{Q}(\mathbf{r}, t)$ is the heat flux density vector along the different axes of the material, κ is the second-rank thermal conductivity tensor, $T(\mathbf{r}, t)$ is temperature gradient as a function of position, $\mathbf{r}$, and time, t. Heat in solids can be transferred via electrons and lattice vibrations (phonons). For the sake of theoretical simplicity electronic heat conduction can be studies as the heat conduction via electrons and holes, spin waves and other excitations. Plasmonic oscillations can also be an important heat transport mechanism in solids. Total thermal conductivity of the material is the algebraic sum of all the thermal conductivity contributions from various mechanisms . The electronic thermal conductivity can be studied using nearly free electron in a periodic potential. This treatment leads to the proof of the Wiedemann-Franz law:

$$L_0 = \frac{\kappa_e}{\sigma T} = 2.4452 \times 10^{-8}\ \mathrm{W\Omega/K^2} \tag{2.2}$$

Here, σ is the electrical conductivity of the material and the numerical value of the Lorentz number L_0 can be calculated in terms of the Boltzmann constant and the electronic charge. The Wiedemann-Franz law typically holds at high temperatures where the inelastic scattering of the charge carriers is relatively insignificant. Pure solid metals such as gold and silver exhibit ignoreable phonon thermal conductivity as the free electrons dominate the thermal conductivity. As we will discuss in the following sections, this is often not the case for the 2D metallic compounds as well as some transition metals and alloys. For the case of semiconducting materials, a similar expression can be derived based on equilibrium distribution of the electrons and

holes. Theoretical treatment of the lattice contribution to the thermal conductivity requires addition of the effects of impurity scattering, isotope effects, etc. However, typically for materials with moderate impurity concentrations the dominant phonon assumption explains the phonon scattering contribution to the thermal conductivity adequately. Of course, discussions for the electronic and phononic thermal conductivity assumes that there are no correlations between the electrons and phonons. This is not entirely true for most of the transition-metal dichalcogenides that we will study in the following sections where electron-phonon correlations lead to intriguing phenomena such as charge density wave transitions. Phonons in a lattice can scatter due to several mechanisms such as phonon-phonon scattering, phonon impurity scattering, phonon-electron scattering and phonon-boundary scattering.

2.2.1 Phonon-Phonon Scattering

Phonon-phonon scattering mechanism can be classified under two categories: the normal process (N-process) that conserves the momentum after scattering and the umklapp (turn-over) process (U-process) that does not conserve the momentum. The U-process is a result of scattering that produces a wave-vector that is larger than the Brillouin zone of the crystal, thus falling into the opposite corner of the Brillouin zone. This literally flips over the momentum of the phonon after the scattering event and as it has ω^2 frequency dependence, it is much more dominant than the N-process with ω dependence at high temperatures for low-defect crystals. The relaxation time, τ_U, for the U-process can be written as:

$$\frac{1}{\tau_U} = 2\gamma^2 \frac{k_B T}{\mu V_0} \frac{\omega^2}{\omega_D} \tag{2.3}$$

where, ω_D is the Debye frequency, γ is the Gruneisen parameter, μ is the shear modulus, V_0 is the volume per atom and ω is the phonon frequency.

Another important thermal relaxation mechanism for low dimensional materials is the boundary scattering. Scattering of phonons from the boundaries of the material leads to thermal resistance when the boundaries are rough. The thermal mean free path, ℓ_B can be written as

$$\ell_B = D \frac{1+p}{1-p} \tag{2.4}$$

where D is the diameter of the sample and p is the specularity parameter. When $p = 1$, the scattering is perfectly specular while $p = 0$ it is perfectly diffusive.

As most of the metallic 2D materials show strong electron-phonon coupling, electron-phonon scattering should also be considered for another thermal resistance mechanism.

$$\frac{1}{\tau_{ph-e}} = \frac{n_e \epsilon^2 \omega}{\rho V^2 k_B T} \sqrt{\frac{\pi m^* V^2}{2 k_B T}} \exp\left(-\frac{m^* V^2}{2 k_B T}\right) \tag{2.5}$$

where n_e is the density of conduction electrons, ϵ is deformation potential, ρ is mass density and $m*$ is effective electron mass.

All the contributions to the thermal relaxation can be added with the Mattheissen's rule as the following:

$$\frac{1}{\tau_{Tot}} = \frac{1}{\tau_U} + \frac{1}{\tau_{ph-e}} + \frac{1}{\tau_B} \tag{2.6}$$

and using the kinetic theory of gasses, it is possible to write a relation between the thermal conductivity and the specific heat, C, phonon group velocity, v, and the thermal relaxation time, τ_{Tot}:

$$\kappa = \frac{1}{3} C v^2 \tau_{Tot} \tag{2.7}$$

Depending on the major heat carriers in the material, the specific heat can be electronic or the lattice.

There are many factors that influence the thermal conduction in materials. Temperature, crystallinity, impurities, defects, carrier density, electron-electron and electron-phonon correlations are a few of these factors. We will discuss the effect of each factor in detail as we discuss specific material families in the following sections. To conclude, I think it is necessary to add that there are various theoretical methods that can be used to obtain the thermal conductivity values such as molecular dynamics simulations besides the analytical approaches we introduced.

2.3 Thermal Conductivity of 2D Materials

2D layered materials exhibit a unique crystal structure that leads to high thermal anisotropy ranging from 50 to 300 slower heat conduction in cross-plane than in-plane [1–3]. The atoms in each layer are covanlently bonded and the layers are stacked via van der Waals interactions. This results in slower heat transport across the layers as compared to the in-plane. Although most of the studies on thermal conductivity of 2D materials are theoretical, there is a good understanding of how heat is carried in these systems both in the monolayer limit as well as in the bulk. In the following subsections I summarize the recent understanding of thermal conduction in 2D materials. I constrained myself to single crystal, single domain properties of each 2D materials family as the composites made up of 2D materials as well as the polycrystalline samples opens up a whole new world for the thermal conductivities. Moreover, conventional methods for such composite and bulk film/crystalline materials are applicable. I limited my attention in this brief to more academic exploration of the 2D materials' thermal properties.

2.3.1 Thermal Conductivity of Graphene

Theory of the thermal conductivity of graphene has been extensively studied in the literature. Thermal conductivity of graphene is mostly due to the phonons as the electronic contribution at room temperature is about 10% of graphene when impurities are excluded. When impurities are included the first-principles calculations, the electronic contribution decreases to 0.5–8 % of the monolayer [4]. Phonons in the graphene can be classified as in-plane and out-of-plane (flexural) modes. Linear transverse acoustic (LA) and longitudinal acoustic (LA) modes are in-plane modes. Flexural modes are acoustic (ZA) and optical (ZO). Seol et al. [5] argued that ZA phonon modes carry most of the heat in graphene due to the large density of ZA flexural phonons resulting from their quadratic dispersion and to a selection rule for three-phonon scattering that arises from the reflection symmetry perpendicular to the graphene plane based on their experimental data. In a follow-up study, using the linearized Boltzmann transport equation Lindsay et al. [6] showed that despite the commonly accepted view, flexural acoustic phonons account for more that 70% of the total thermal conductivity [7]. Thus the choice of substrate is very important (see Fig. 2.1). This is also similar in h-BN [7]. For the cross-plane thermal transport a key quantity is the phonon mean free path. Molecular dynamics simulations and experimental measurements of the cross-plane thermal transport measurements showed that the phonon mean free path can be on the order of hundreds of nanometers [8–10]. Another important factor in the thermal conductivity of graphene is the isotope effect [11].

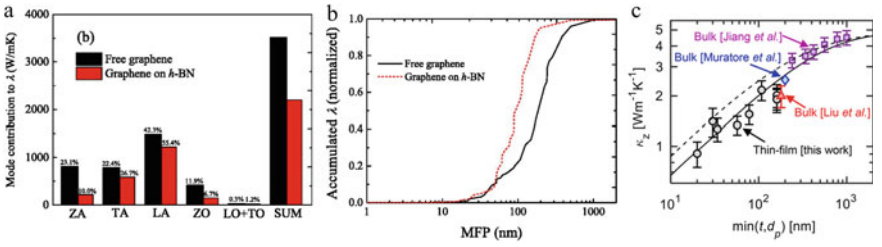

Fig. 2.1 **a**. Mode thermal conductivity of free and supported graphene calculated using molecular dynamics simulations showing the effect of substrate on the thermal properties. **b**. Figure shows the accumulative thermal conductivity as a function of the phonon mean free path in graphene and graphene on h-BN from molecular dynamics simulations. The figure is reprinted with the permission from Zou et al. [12]. Copyright (2017) AIP Publishing. **c**. Cross-plane thermal conductivity of MoS_2 as a function of thickness. The figure is reprinted with the permission from Sood et al. [13]. Copyright (2019) American Chemical Society

2.3.2 Thermal Conductivity of TMDCs

MoS_2 has been a prototypical material for TMDC studies due to ease of synthesis and high quality mined crystals. Thus, most thermal conductivity studies of TMDCs are focused on MoS_2. However, both experimentally and computationally there are large discrepancies in the thermal conductivity values reported on MoS_2. In-plane thermal conductivity values are in the range of 44–52 $Wm^{-1}K^{-1}$ [14, 15]. Of course the discrepancy might arise from the differences in the crystal thicknesses. Cross-plane thermal conductivity is also strongly effected by the thickness of the crystals due to very long phonon mean free paths along the z-axis [13]. From 20 to 1000 nm cross-plane thermal conductivity increases from 1 to 4 $Wm^{-1}K^{-1}$ as shown in Fig. 2.1 [3, 13, 16, 17].

Thermal conductivity can be greatly modified by the isotope effect similar to graphene. As an instance, it has been demonstrated that the thermal conductivity of MoS_2 prepared with ^{100}Mo isotope shows 50% enhanced thermal conductivity compared with the MoS_2 prepared with naturally occurring Mo isotopes [18]. This enhancement is attributed to the combined effects of reduced isotopic disorder and a reduction in defect-related scattering mechanisms.

2.3.3 Thermal Conductivity of Heterostructures

The heterostructures of 2D materials are very promising for enabling new applications using features that are not existent in the pristine materials [19]. There has been limited interest in the thermal conductivity of the heterostructures. Gao et al. theoretically studied the graphene-MoS_2 heterostructure using nonequilibrium molecular dynamics simulations and showed that the heterostructure has a lower thermal conductivity that decreases further with strain than graphene but higher than MoS_2 monolayer [20]. A similar feature is also demonstrated in perfect $MoS_2/MoSe_2$ heterostructures [21]. Beyond these studies, as discussed before, graphene on h-BN has been studied to a certain extend. There is still a lot to be done on the heterostructures of 2D materials.

2.4 Thermal Conductivity Measurement Methods in 2D Materials

Thermal conductivity measurements requires the measurement of heat transferred over the sample and measuring temperature is the most straightforward way to extract this information. However, measuring the temperature is not always straightforward. The problem is two-fold. First, if the sample size is very small, measuring the temperature requires a sensitive senor to probe the temperature, which complicates the

device fabrication significantly. Second, as it is nearly impossible to fully isolate a material from its surrounding thermally, the heat transferred through other paths also has to be taken into the account. As the focus in this brief is on 2D materials, I would like to discuss the most commonly used methods on 2D materials.

Thermal conductivity measurement methods can be classified under two sections depending on the thermal equilibrium of the sample under measurement: transient methods and steady-state methods. In transient methods, thermal conductivity is measured in time (or frequency) domain when the thermal equilibrium has not reached with the surroundings. Most commonly used transient methods are the time-domain thermoreflectance spectroscopy and the 3ω method. In the steady-state methods, thermal equilibrium is established for the measurements. Most commonly used steady-state methods are the Raman thermometry based thermal conductivity measurement method, micro-bridge method. The method we introduced recently based on the bolometric effect is also a steady-state method. We will discuss all these methods in detail with their applicability in 2D materials.

2.4.1 Raman Thermometry

Raman spectroscopy is a versatile tool for materials characterization as the specific vibrational Raman active modes provide valuable information about the material. Some of the Raman active modes are sensitive to external influences such as strain, temperature and doping of the material. These external influences modify the stiffness among the constituent elements forming the material, thus leading to an observable shifts in the Raman spectrum. Raman thermometry is based on the temperature dependent shifts of the Raman active shifts. Thus, under sufficiently low laser illumination, it is possible to use the Raman shift as a thermometer [22, 23]. Although the method has been proposed to be used on silicon, it became very popular after being used to measure the thermal conductivity of graphene [24].

To be used in 2D materials, substrate preparation is mandatory. A substrate with circular holes are etched on the substrate and the nanosheet is transferred over the holes to suspend a certain section of the crystal. Then, a diffraction-limited laser spot is positioned over the center of the hole to measure the Raman spectrum at the lowest possible laser power at different substrate temperatures, T_{sub}. This provides the first-order temperature coefficient of Raman peak shift, $\chi_T = \Delta\omega/(T_2 - T_1)$. Typically, this parameter has to be measured over a very wide temperature range to get an accurate slope for χ_T. For instance, the plot shows a typical data set for MoS_2 adapted from Sahoo et al. [14], Yan et al. [25] and Zhang et al. [26] shows that a reliable slope can be extracted over a temperature range of 200 K. When the slope is measured in a narrower temperature range, the uncertainty in the slope becomes so large that the measured thermal conductivity value ranges significantly. Once χ_T is measured, the next step is the measurement of χ_P that is the Raman peak shift with the absorbed laser power. First of all, absorbance for the material under investigation has to be carefully measured. It should be also noted that the absorption can vary with

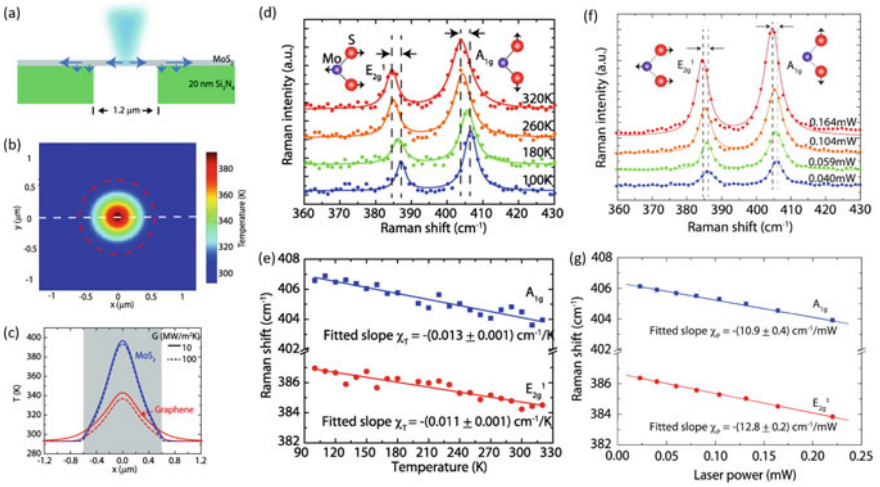

Fig. 2.2 **a**. Schematic of the side view of an MoS_2 crystal suspended over a hole with laser illumination from the top. Thermal simulation showing the heat distribution over the suspended and the supported parts of the crystal. **c**. Comparison of thermal distribution of graphene and MoS_2 monolayer under the same laser illumination at different thermal boundary conductance values. **d**. Raman peak shifts at various temperatures shown as the full spectrum and e. peak position shifts at various temperatures as a plot. **e**. Raman peak shifts as a function of the laser power shown as the full spectrum and **f**. peak shits at various powers. All the figures are reprinted with the permission from Yan et al. [25]. Copyright (2014) American Chemical Society

the temperature. Another consideration is the fact that the laser spot has a Gaussian power distribution, thus the local temperature distribution has to be weighted by the Gaussian profile of the laser spot. Thus, with the known mean temperature under the laser spot, the heat equation for the suspended and the supported part can be solved to give the thermal conductivity. The method is employed on various thin layers such as $MoSe_2$ [26, 27], WS_2 [28] (Fig. 2.2)

The method stands out as an exceptionally easy to implement method among the other thermal conductivity measurement methods that are applicable to 2D materials. This is mostly due to the simplicity of device fabrication and the experimental setup. Also, the analysis of the obtained data is much more simpler compared to the TDTR or 3ω methods. However, there are serious limitations of the method as well.

2.4.1.1 Limitations of the Raman Thermometry

Based on the first-principles calculations Vallabhaneni et al. [29] showed that different phonon polarizations are not in thermal equilibrium in graphene. This is the the well-accepted assumption of the Raman method. As a result, the method underestimates the thermal conductivity by a factor of 1.35–2.6. Further, they claim that such an underestimation is expected for other 2D materials when the optical-acoustic phonon coupling is weak.

Another limitation of the method is the requirement of having a Raman peak that is insensitive to the pre-tension due to suspension of the crystals over the hole. As it is very well known from the indentation experiments [30], there is a built-in stress to the stretched membrane over the hole. Thus, it is imperative to choose a peak that is relatively insensitive to the stretching of the crystal but with high enough χ_T. For most materials the thermal conductivity measurement can be performed with a 10 K average temperature increase. As an example χ_T for MoS_2 is about $-0.013\,cm^{-1}/K$. A very long focal length spectrometer equipped with a cutting-edge spectrometer, the resolution is limited to $0.5\,cm^{-1}$. Lorentzian fitting to the Raman peak can improve the peak position detection sensitivity to $0.25\,cm^{-1}$. Still, such a sensitivity requires 20 K of average temperature increase over the hole. Such a temperature rise might be very important in the study of materials that show temperature dependent phase transitions.

Absorbance of the laser power by the sample is another point that requires attention. As the calculation of the thermal conductivity depends on the laser power absorbed by the material, absorbance of the material has to be determined. Moreover, in most cases the hole under the sample is not a through hole and the light scattered from its base also contributes to the heating of the sample. Other limitations might also arise from the experimental setup. As an instance, positioning of the laser spot at the center of the suspended part is important. Any inaccuracy in the positioning of the laser spot will lead to large errors in thermal conductivity value for small radius holes. Another experimentally important aspect of the measurement is the beam profiling. Gaussian laser spot has to be profiled to extract the full-width-half-maximum.

2.4.2 Micro-Bridge Thermometry

Micro-bridge thermometry is an absolute thermal conductivity measurement method that relies on thermal isolation of the sample from the surrounding and delivering a measurable amount of heat from one side of the sample to the other while measuring the temperature of the sample at both sides. SEM images of the experimental configuration and the equivalent thermal circuit is given in Fig. 2.3. The method has been applied on measuring the thermal properties of multi-wall carbon nanotubes by Kim et al. [31]. The method has been then adapted for 2D materials. The method has been applied on graphene [5, 32–35], h-BN [36], MoS_2 [15] and black phosphorus [37].

2.4.2.1 Limitations of the Micro-Bridge Thermometry

Despite the versatility of the micro-bridge thermometry, implementation of the method is very difficult especially on 2D materials. Most of the studies cited for the micro-bridge thermometry uses either thick crystals or they require very stiff materials like graphene and h-BN to survive the intense device fabrication procedures.

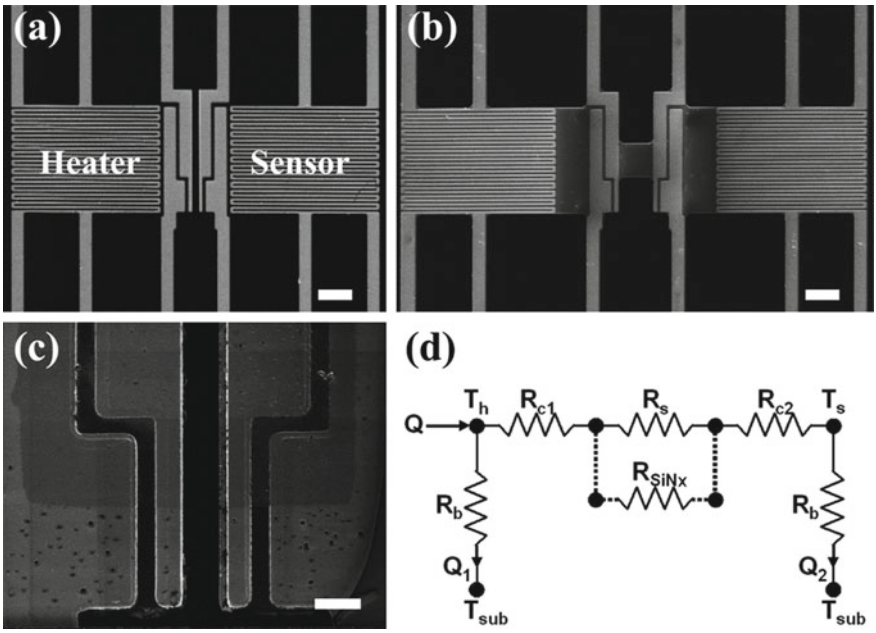

Fig. 2.3 Figure copied from Wang et al. [32] showing SEM micrographs of **a**. the micro-bridge structures with heater and the sensor parts, **b**. with the graphene flake suspended across the the pads and **c**. a close-up image of the contact pads. d. Equivalent thermal circuit of the device is shown. Scale bars are 5 μm for a and b, 1 μm for c. Reprinted with permission from Wang et al. [32]. Copyright (2011) American Chemical Society

Device fabrication steps including many lithography and etching also leads to significant contamination of the crystals, resulting in significant changes in the thermal properties due to the scattering of the phonons from the polymeric residues [32, 33]. Thus, the widespread use of the method is not possible. Moreover, similar to the Raman thermometry the stress on the crystal further complicates the analysis of the measurements. Perhaps, this is common to the all thermal conductivity measurement methods, yet for the sake of completeness we should also mention that it is not entirely possible to isolate the heating pads from the surrounding. As a result, the heat lost to the connections is very difficult to account for, leading to further uncertainties.

2.4.3 Scanning Thermal Microscopy

Scanning thermal microscopy (SThM) is a variant of AFM that is modified to measure the local temperature over the sample. Typically, the AFM tip is made of Pt-Cr junction to be used as a thermocouple that is overlayed on one another with separation

terminated near the tip. The method first introduced by Majumdar and his group [38–40]. It is possible to measure the temperature distribution with a spatial resolution of 100 nm, that is more than twice better than the Raman thermometry. A quantitative measurement of the temperature, of course, requires a very careful analysis of all the possible heat loss mechanisms and interaction of the tip with substrate. Due to these complications it has not been widely used in the thermal conductivity measurements of 2D materials (Fig. 2.4).

2.4.4 Time-Domain Thermoreflectance Method

Time-domain thermoreflectance (TDTR) method uses the reflectance change of the material upon heating to measure the thermal conductivity via intense modelling. The method is a pump-probe spectroscopy in essence. An ultra-fast laser pulse sent on to the sample to create a local temperature rise due to optical absorption and then the second pulse, probes the reflection change of the sample. The time when the probe pulse with respect to the pulse arrives on the sample can provide how the heat is dissipated over the sample in time. The method is introduced by Paddock et al. [42] to measure the thermal diffusivity of metallic films. The laser spot is focused to a 20 μm in the original work and given the fact that the heat diffusion within a few hundred picoseconds can only reach a fraction of the laser spot, the model assumes a one-dimensional diffusion in to the sample. The heat diffusion length $l \approx \sqrt{h\tau}$ where h is the thermal diffusivity and τ is the time after the arrival of the heating pulse. For a typical metal with 200 ps delay between the pump and the probe, $l \approx 50$ nm. If the sample thickness is restricted below l then, effectively the problem is a 1D heat diffusion problem.

The method can be used to measure not only the thermal diffusivity of the sample but thermal properties of materials in general such as thermal conductivity [44, 45], the thermal conductance of interfaces [46, 47], microfabricated structures etc. [48]. To measure the thermal properties of 2D materials, a highly thermoreflective coating such as aluminium has to applied on semiconducting crystals. Besides having high thermoreflectance, Al has a linear dependence of reflactance to the surface temperature change. As 2D materials are highly anisotropic in in-plane and out-of-plane directions, one-dimensional model proposed above is not applicable to 2D materials. Further the interface between the Al layer and the 2D material has to be taken in to account.

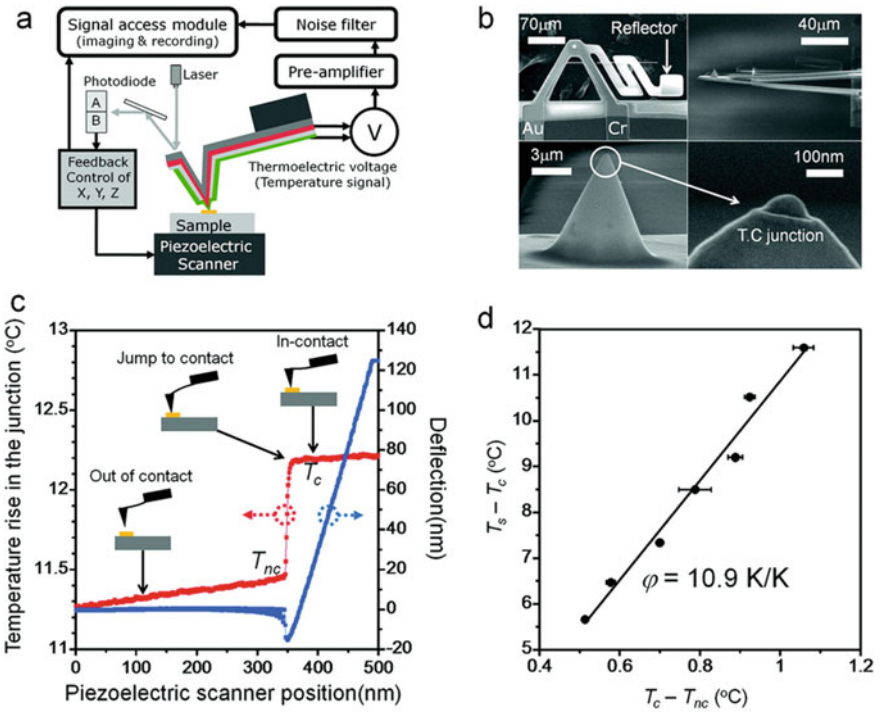

Fig. 2.4 Figure copied from Kim et al. [41] showing the details of the SThM method and their measurements. **a**. Schematic of the SThM operation. **b**. SEM micrographs of the AFM tip used by Kim et al. [41] **c**. Temperature rise at the junction with respect to the piezo position as well as the deflection of the tip versus the piezo position is given. Upon contact with the substrate, the temperature rises by almost a Kelvin. **d**. Difference between the sample temperature T_s and the contact temperature T_c versus the difference between T_c and the non-contact temperature T_nc gives the dimensionless constant ϕ for the particular tip. The figure is reprinted with permission from Kim et al. [41]. Copyright (2011) American Chemical Society

2.4.4.1 Limitations of the TDTR Method

The major limitation of TDTR method is that it cannot be really applied on 2D materials.[1] First of all, a minimum sample thickness of 20 nm is required for acquiring the thermal properties of the material. This comes at the cost of having cross-plane heat transport, which is highly different than the in-plane thermal transport in 2D materials due to the weak interlayer coupling. Jiang et al. [16] measured the in-plane and cross-plane thermal conductivities of MX_2 (M = Mo, W and X = S, Se) bulk crystals using TDTR technique using a variable-spot-size approach [49] and showed that there is nearly two orders of magnitude difference in cross-plane and in-plane

[1] Unless the purpose is to study the the cross-plane thermal conductivity, then TDTR is superior to all techniques especially with the recent improvements as discussed later.

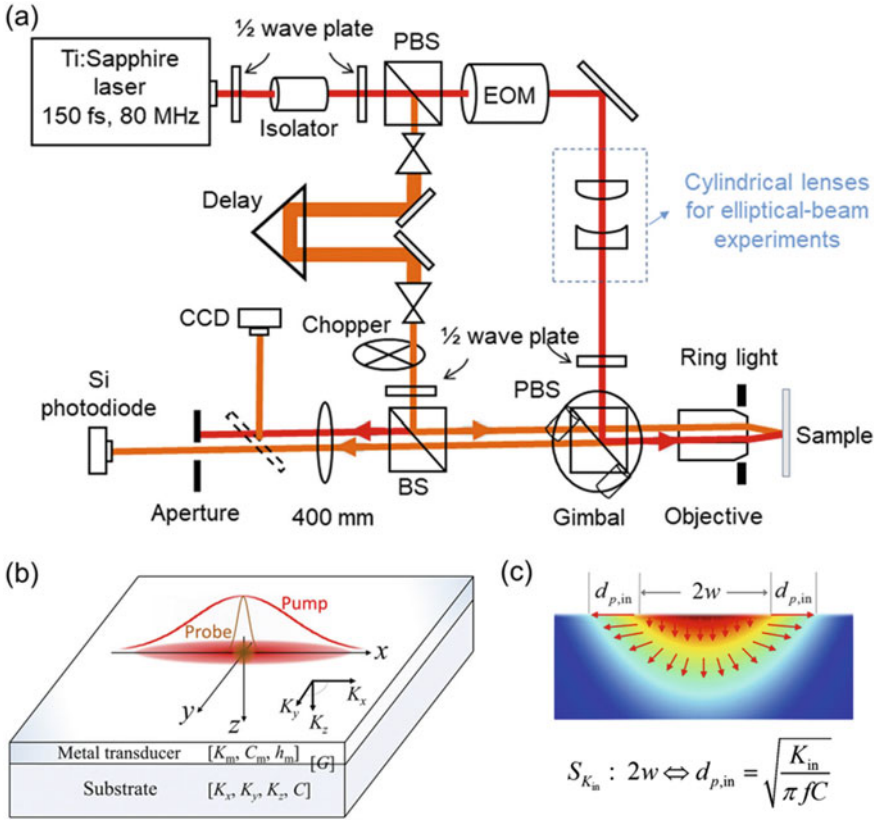

Fig. 2.5 **a**. Schematic showing the experimental setup for the TDTR method. EOM, PBS, and BS stand for electro-optic modulator, polarizing beam splitter, and beam splitter, respectively. **b**. Schematic showing how elliptical-beam method works on the sample. **c**. Heat flux directions and the comparison of the laser spot size to the sample depth. Figure is reprinted with the permission of Jiang et al. [43]. Copyright (2018) AIP Publishing

thermal conductivity values. The method is also applied on bulk black phosphorus [50], graphene and h-BN [49]. Finally, the very expensive and highly customized experimental setup makes the technique inaccessible to widespread use (Fig. 2.5).

2.4.5 3ω Method

The method requires a narrow metal line to be placed on the material to be measured, typically prepared by lithography followed by metal evaporation. This metal line serves both as the heater and the thermometer for the measurements. An ac current at 2ω is applied to the metal to cause Joule heating. This results in temperature

oscillations of the metal line at frequency 2ω and as a result the resistance change of the metal can be detected at the third harmonic 3ω. To my best knowledge, the method has not been applied to 2D materials due to the insensitivity of method to the in-plane and cross-plane thermal conductivity. However, I wanted to include it among the measurement techniques as it is potentially applicable to atomically thin isotropic materials.

2.4.6 Bolometry Based Method

In a recent study, we introduced a novel method to measure thermal conductivity in 2D materials, in particular the metallic ones based on the bolometric effect [51]. In Chap. 3, I provide a very detailed description of the method with many details. Here, I wanted to introduce the method very briefly to give a background for the comparison table for the thermal conductivity methods that I provided in the next subsection. In essence the bolometry based thermal conductivity measurement method is very similar to the Raman thermometry based thermal conductivity measurement method.

2.4.7 Comparison of Thermal Conductivity Measurement Methods

I have to state that there is no single "best thermal conductivity measurement method" as all the techniques mentioned are superior to others in certain aspects. Thus, I would like to compare different thermal conductivity measurement methods not to find a better method but to demonstrate their domains of applicability. Moreover, it should be noted that a particular choice of the measurement method may extend beyond simply measuring the thermal conductivity of a material and to study various thermal properties of a material. For that matter, Raman thermometry has been the simplest choice for many researchers due to the ease of applicability to 2D materials thanks to very simple sample preparation that only requires the transfer of 2D flake over pre-drilled holes on the substrate. Although the experimental setup is rather complicated, micro-Raman setups are widely available in many research laboratories. One has to integrate a cooling or an heating stage as well. Moreover, a fine diffraction grating is required (typically something beyond 1200 lines/mm) to have a good spectral resolution. However, the method suffers from low accuracy and low sensitivity. Moreover, a moderate amount of data analysis is required to extract the thermal conductivity value. Method only works for in-plane measurements. In-plane anisotropy can be measured with a line profiled laser spot. TDTR method is a well established method that has been used very frequently in the study of thermal conductivity in many materials. However, its applicability to 2D materials is limited to cross-plane measurements. The greatest drawback of the method is the vast complexity of the

Method / Attribute	Raman Thermometry	TDTR	Micro-Bridge Thermometry	Bolometry Based Thermometry
Applicability to 2D Materials	Applicable	Applicable in bulk	Limited Applicablility	Applicable
Ease of Sample Preparation	Easy	Moderate	Very Difficult	Moderate
Experimental Setup	Complicated	Very Complicated	Very Complicated	Complicated
Accuracy	Low	High	Very High	High
Sensitivity	Low	High	Very High	High
Data Analysis	Moderate	Intensive	Simple	Simple

Fig. 2.6 A qualitative comparison table to compare different thermal conductivity measurement methods. Details of the bolometry based thermometry is explained in Chap. 3

measurement setup. In essence it is a pump-probe spectroscopy that requires an ultrafast laser with delay lines and many optical components. Also, it requires intensive data analysis to extract the thermal properties of the material. It provides high sensitivity and high accuracy compared to other methods. Micro-bridge thermometry method has rather limited applicability to 2D materials manly due to very difficult device fabrication steps. Moreover, the experimental setup for the measurement are relatively complicated. It provides very simple data analysis with very high accuracy and sensitivity. Details of the bolometry based thermometry is given in Chap. 3. To summarize, it is highly applicable to 2D materials that shows limited photovoltaic photoresponse. Sample preparation is slightly more difficult than the Raman thermometry as it requires fabrication of metal contacts on the substrate. Experimental setup is fairly complicated as the measurement requires a current pre-amplifier attached to a lock-in amplifier. It provides high accuracy with very high sensitivity. Data analysis is also simple. Figure 2.6 gives a table for a comparison of the methods.

References

1. Sichel EK, Miller RE, Abrahams MS, Buiocchi CJ (1976) Phys Rev B 13(10):4607. https://link.aps.org/doi/10.1103/PhysRevB.13.4607
2. Schmidt AJ, Chen X, Chen G (2008) Rev Sci Instrum 79(11):114902. http://aip.scitation.org/doi/10.1063/1.3006335
3. Liu J, Choi GM, Cahill DG (2014) J Appl Phys 116(23):233107. http://dx.doi.org/10.1063/1.4904513, http://aip.scitation.org/doi/10.1063/1.4904513

4. Kim TY, Park CH, Marzari N (2016) Nano Lett 16(4):2439. https://doi.org/10.1021/acs.nanolett.5b05288
5. Seol JH, Jo I, Moore AL, Lindsay L, Aitken ZH, Pettes MT, Li X, Yao Z, Huang R, Broido D, Mingo N, Ruoff RS, Shi L (2010) Science 328(5975):213. https://www.sciencemag.org/lookup/doi/10.1126/science.1184014
6. Lindsay L, Broido DA, Mingo N (2010) Phys Rev B 82(11):115427. https://link.aps.org/doi/10.1103/PhysRevB.82.115427
7. Lindsay L, Li W, Carrete J, Mingo N, Broido DA, Reinecke TL (2014) Phys Rev B 89(15):155426. https://link.aps.org/doi/10.1103/PhysRevB.89.155426
8. Wei Z, Yang J, Chen W, Bi K, Li D, Chen Y (2014) Appl Phys Lett 104(8):081903. http://aip.scitation.org/doi/10.1063/1.4866416
9. Fu Q, Yang J, Chen Y, Li D, Xu D (2015) Appl Phys Lett 106:3. http://dx.doi.org/10.1063/1.4906348
10. Zhang H, Chen X, Jho YD, Minnich AJ (2016) Nano Lett 16(3):1643. https://pubs.acs.org/doi/10.1021/acs.nanolett.5b04499
11. Chen S, Wu Q, Mishra C, Kang J, Zhang H, Cho K, Cai W, Balandin AA, Ruoff RS (2012) Nat Mater 11(3):203. http://dx.doi.org/10.1038/nmat3207, http://www.nature.com/articles/nmat3207
12. Zou JH, Cao BY (2017) Appl Phys Lett 110(10):103106. https://doi.org/10.1063/1.4978434.
13. Sood A, Xiong F, Chen S, Cheaito R, Lian F, Asheghi M, Cui Y, Donadio D, Goodson KE, Pop E (2019) Nano Lett 19(4):2434. https://doi.org/10.1021/acs.nanolett.8b05174
14. Sahoo S, Gaur AP, Ahmadi M, Guinel MJ, Katiyar RS (2013) J Phys Chem C 117(17):9042. https://doi.org/10.1021/jp402509w
15. Jo I, Pettes MT, Ou E, Wu W, Shi L (2014) Appl Phys Lett 104:20. http://dx.doi.org/10.1063/1.4876965
16. Jiang P, Qian X, Gu X, Yang R (2017) Adv Mater 29(36):1. https://doi.org/10.1002/adma.201701068
17. Muratore C, Varshney V, Gengler JJ, Hu JJ, Bultman JE, Smith TM, Shamberger PJ, Qiu B, Ruan X, Roy AK, Voevodin AA (2013) Appl Phys Lett 102(8):081604. http://aip.scitation.org/doi/10.1063/1.4793203
18. Li X, Zhang J, Puretzky AA, Yoshimura A, Sang X, Cui Q, Li Y, Liang L, Ghosh AW, Zhao H, Unocic RR, Meunier V, Rouleau CM, Sumpter BG, Geohegan DB, Xiao K (2019) ACS Nano 13(2). https://pubs.acs.org/doi/10.1021/acsnano.8b09448
19. Cao Y, Fatemi V, Fang S, Watanabe K, Taniguchi T, Kaxiras E, Jarillo-Herrero P (2018) Nature 556(7699):43. https://doi.org/10.1038/nature26160
20. Gao Y, Liu Q, Xu B (2016) ACS Nano 10(5):5431. https://pubs.acs.org/doi/10.1021/acsnano.6b01674
21. Zheng X, Zhao C, Gu X (2019) Int J Heat Mass Transf 143:118583. https://doi.org/10.1016/j.ijheatmasstransfer.2019.118583, https://linkinghub.elsevier.com/retrieve/pii/S0017931019323312
22. Périchon S, Lysenko V, Remaki B, Barbier D, Champagnon B (1999) J Appl Phys 86(8):4700. https://doi.org/10.1063/1.371424
23. Périchon P, Lysenko V, Roussel P, Remaki B, Champagnon B, Barbier D, Pinard P (2000) Sens Actuators A Phys 85(1):335. https://doi.org/10.1016/S0924-4247(00)00327-7
24. Balandin AA, Ghosh S, Bao W, Calizo I, Teweldebrhan D, Miao F, Lau CN (2008) Nano Lett 8(3):902. https://doi.org/10.1021/nl0731872
25. Yan R, Simpson JR, Bertolazzi S, Brivio J, Watson M, Wu X, Kis A, Luo T, Hight Walker AR, Xing HG (2014) ACS Nano. 8(1):986. https://doi.org/10.1021/nn405826k
26. Zhang X, Sun D, Li Y, Lee GH, Cui X, Chenet D, You Y, Heinz TF, Hone JC (2015) ACS Appl Mater Interfaces 7(46):25923. https://doi.org/10.1021/acsami.5b08580
27. Wang R, Wang T, Zobeiri H, Yuan P, Deng C, Yue Y, Xu S, Wang X (2018) Nanoscale 10(48):23087. https://doi.org/10.1039/c8nr05641b
28. Peimyoo N, Shang J, Yang W, Wang Y, Cong C, Yu T (2015) Nano Res 8(4):1210. https://doi.org/10.1007/s12274-014-0602-0

29. Vallabhaneni AK, Singh D, Bao H, Murthy J, Ruan X (2016) Phys Rev B 93(12):1. https://doi.org/10.1103/PhysRevB.93.125432
30. Lee C, Wei X, Kysar JW, Hone J (2008) Science 321(5887):385. https://www.sciencemag.org/lookup/doi/10.1126/science.1157996
31. Kim P, Shi L, Majumdar A, McEuen PL (2001) Phys Rev Lett 87(21):215502. https://doi.org/10.1103/PhysRevLett.87.215502
32. Wang Z, Xie R, Bui CT, Liu D, Ni X, Li B, Thong JT (2011) Nano Lett 11(1):113. https://doi.org/10.1021/nl102923q
33. Pettes MT, Jo I, Yao Z, Shi L (2011) Nano Lett 11(3):1195. https://doi.org/10.1021/nl104156y
34. Jang W, Bao W, Jing L, Lau CN, Dames C (2013) Appl Phys Lett 103(13):6. https://doi.org/10.1063/1.4821941
35. Xu X, Pereira LF, Wang Y, Wu J, Zhang K, Zhao X, Bae S, Tinh Bui C, Xie R, Thong JT, Hong BH, Loh KP, Donadio D, Li B, Özyilmaz B (2014) Nat Commun 5:1. https://doi.org/10.1038/ncomms4689
36. Jo I, Pettes MT, Kim J, Watanabe K, Taniguchi T, Yao Z, Shi L (2013) Nano Lett 13(2):550. https://doi.org/10.1021/nl304060g
37. Lee S, Yang F, Suh J, Yang S, Lee Y, Li G, Choe HS, Suslu A, Chen Y, Ko C, Park J, Liu K, Li J, Hippalgaonkar K, Urban JJ, Tongay S, Wu J (2015) Nat Commun 6. https://doi.org/10.1038/ncomms9573
38. Majumdar A (1999) Annu Rev Mater Sci 29(1):505. http://www.annualreviews.org/doi/10.1146/annurev.matsci.29.1.505
39. Shi L, Plyasunov S, Bachtold A, McEuen PL, Majumdar A (2000) Appl Phys Lett 77(26):4295. http://aip.scitation.org/doi/10.1063/1.1334658
40. Shi L, Majumdar A (2002) J Heat Transf 124(2):329. https://doi.org/10.1115/1.1447939
41. Kim K, Chung J, Hwang G, Kwon O, Lee JS (2011) ACS Nano 5(11):8700. https://doi.org/10.1021/nn2026325
42. Paddock CA, Eesley GL (1986) J Appl Phys 60(1):285. https://doi.org/10.1063/1.337642
43. Jiang P, Qian X, Yang R (2018) Rev Sci Instrum 89(9):094902. http://aip.scitation.org/doi/10.1063/1.5029971
44. Cahill DG, Goodson K, Majumdar A (2002) J Heat Transf 124(2):223. https://doi.org/10.1115/1.1454111
45. Cahill DG, Ford WK, Goodson KE, Mahan GD, Majumdar A, Maris HJ, Merlin R, Phillpot SR (2003) J Appl Phys 93(2):793. https://doi.org/10.1063/1.1524305
46. Costescu RM, Wall MA, Cahill DG (2003) Phys Rev B Condens Matter Mater Phys 67(5):1. https://doi.org/10.1103/PhysRevB.67.054302
47. Costescu RM, Cahill DG, Fabreguette FH, Sechrist ZA, George SM (2004) Science 303(5660):989. https://www.sciencemag.org/lookup/doi/10.1126/science.1093711
48. Huxtable ST, Cahill DG, Phinney LM (2004) J Appl Phys 95(4):2102. https://doi.org/10.1063/1.1639146
49. Jiang P, Qian X, Yang R (2017) Rev Sci Instrum 88:7. http://dx.doi.org/10.1063/1.4991715
50. Jang H, Wood JD, Ryder CR, Hersam MC, Cahill DG (2015) Adv Mater 27(48):8017. https://doi.org/10.1002/adma.201503466
51. Cakiroglu O, Mehmood N, Çiçek MM, Aikebaier A, Rasouli HR, Durgun E, Kasirga ST (2016) 2D Mater 11(2020). https://iopscience.iop.org/article/10.1088/2053-1583/ab8048